International Journal of Advanced Research in Physical Science (IJARPS)
Volume 10, Issue 7, 2023, PP 5-20
ISSN No. (Online) 2349-7882
www.arcjournals.org

To Question about Nature of Laser-Induced Explosive Processes and Phenomena

Petro P. Trokhimchuck*

Anatoliy Svidzinskiy Department of Theoretical and Computer Physics, Lesya Ukrayinka Volyn' National University, 13 Voly Avenue, 43025, Lutsk, Ukraine, Trokhimchuck

Corresponding Author:** ***Petro P. Trokhimchuck, *Anatoliy Svidzinskiy Department of Theoretical and Computer Physics, Lesya Ukrayinka Volyn' National University, 13 Voly Avenue, 43025, Lutsk, Ukraine, Trokhimchuck*

Abstract: *Main peculiarities of laser-induced explosive processes and phenomena are discussing. Short review of corresponding experimental data is representing. Corresponding models and theories, which are used for the explanation these processes and phenomena p, are represented. Some peculiarities of microscopic aspects of these processes are observing. Comparative analysis of classical, including cumulative, explosion theory is discussing.*

The given models make it possible to explain the corresponding experimental data.

Keywords: *explosive process, Relaxed Optics, acoustic, cascade processes, laser irradiation, filaments, liquids, solid.*

1. INTRODUCTION

Various aspects of the laser-induced explosion, including its relationship with other theories and explosion phenomena, are presented in [1 – 36].

The problem of explosion is connecteds with comcept of detonation.

Detonation is a type of combustion involving a supersonic exothermic front accelerating through a medium that eventually drives a shock front propagating directly in front of it [4]. Detonations propagate supersonically through shock waves with speeds in the range of 1 km/sec and differ from deflagrations which have subsonic flame speeds in the range of 1 *m*/*sec*.

Detonations occur in both conventional solid and liquid explosives,[3] as well as in reactive gases. The velocity of detonation in solid and liquid explosives is much higher than that in gaseous ones, which allows the wave system to be observed with greater detail (higher resolution).

A very wide variety of fuels may occur as gases (e.g. hydrogen), droplet fogs, or dust suspensions. In addition to dioxygen, oxidants can include halogen compounds, ozone, hydrogen peroxide and oxides of nitrogen. Gaseous detonations are often associated with a mixture of fuel and oxidant in a composition somewhat below conventional flammability ratios. They happen most often in confined systems, but they sometimes occur in large vapor clouds. Other materials, such as acetylene, ozone, and hydrogen peroxide are detonable in the absence of an oxidant (or reductant). In these cases the energy released results from the rearrangement of the molecular constituents of the material [4].

Detonation was discovered in 1881 by four French scientists Marcellin Berthelot and Paul Marie Eugène Vieille[6] and Ernest-François Mallard and Henry Louis Le Chatelier [4]. The mathematical predictions of propagation were carried out first by David Chapman in 1899 [4] and by Émile Jouguet in 1905, 1906 and 1917 [4]. The next advance in understanding detonation was made by John von Neumann] and Werner Döring in the early 1940s and Yakov B. Zel'dovich and Aleksandr Solomonovich Kompaneets in the 1960s [4].

From a physical-chemical point of view, an explosion is understood as a set of chemical reactions, the speed of which is greater than the speed of sound. In other words, the intensity of the explosion depends on the Mach number. At the same time, the problem of saturation of the reaction plays an important role, in other words, it is necessary that all the available substance take part in the reaction in a time shorter than the time of the explosion. It is from

this point of view that a laser-induced explosion should be considered. For the laser case, it is necessary that the chain of relevant processes, including the transformation of radiation and the irradiated substance, is in the zone of spatio-temporal coherence.

Explosive-type processes include a part of ablation (laser-induced sputtering) and optical breakdown processes [11, 12].

The problem of critical laser-induced processes and phenomena have large value for development of Nonlinear and Relaxed Optics and physics of dynamical irreversible processes [11 – 15].

Rough short pressure scale and time scale under dynamic loading is representing in Fig. 1 [32].

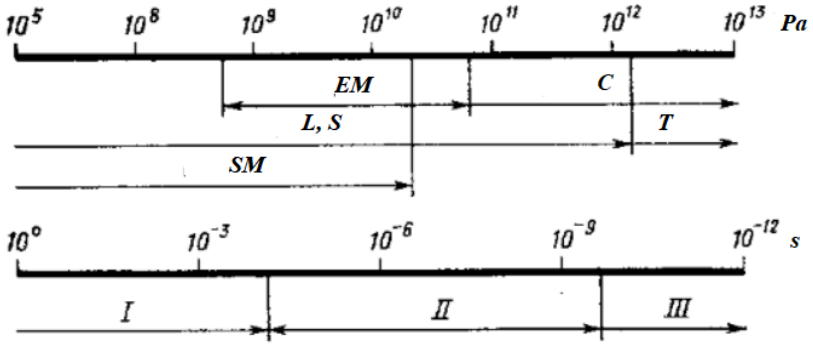

Fig1. *Pressure scale and time scale under dynamic loading: EM – explosive methods; C – cumulation; L and S – laser and shock impact; SM – statistical methods; T – thermonuclear processes; I – throwing bodies by combustion products; II – detonation processes, propagation of shock waves in dense (liquids and solids) media, throwing bodies by explosion, dynamic destruction; III – thermonuclear processes and meteorite impac [32].*

Schema of Fig. 1 give qualitative pictures of main laser-induced shork and explosive processes. However, we have various peculiarities, which are changing geometrical and physical nature of thes phenomena. So, critical phenomena may be have acoustic and electromagnetic nature, irradiation or other experimental conditions may be changing temporal and spatial characteristics of corresponding processes and phenomena.

Generalizing conditional phase diagram is representing in Fig. 2 [32]. This diagram is very rough because it is not including microscopic mechanisms and cascade of laser-induced processes, which are allow receiving of finish picture.

Directed explosive processes may be of two types:

1. Processes, which are determing of procedure of irradiation and further development of cascade corresponding processes. These processes may be calling as inner processes.

2. Proceses, which are determing of geometry of corresponding experiment. These processes may be calling as external processes.

Example of first type processes may be laser-induced breakdown of matter. Example of second type processes may be cumulative explosion [32].

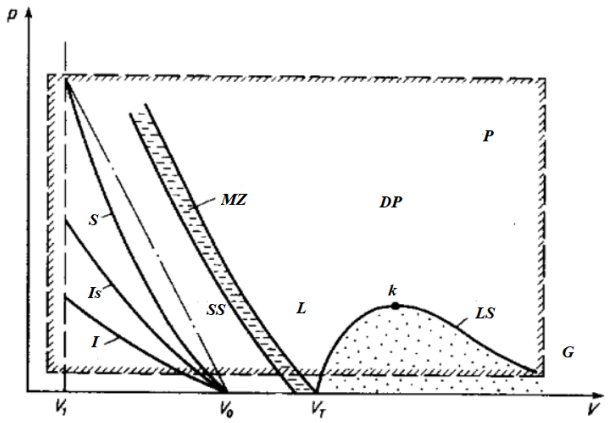

Fig2. *Conditional phase diagram: I – isotherm; Is – isentrope; S – shock adiabat; SS – solid state; MZ – melting zone; L – liquid; V_T – triple point; k – critical point; LS – liquid-steam equilibrium curve (boiling curve); G – gas; PP DP – dense plasma; P – plasma [32].*

2. EXPERIMENTAL DATA

In order to correlate the material properties with the laser parameters, a nondimensional absorption parameter *B* has been developed' and is defined as [3]

$$B = {KbL_v}/{IC_p}, \quad (1)$$

where *K* is the thermal conductivity, *b* the absorption coefficient, *L* the heat of vaporization, I the laser intensity, and C_p the heat capacity.

Figures 3(a) and 3(b) are illustrative of the results obtained using a high speed framing camera. These photographs are each representative of a single frame from a strip of film (one run of the camera) containing twenty-five frames. Color film has been used for framing rates up to 250,000 frames/sec in order that ionization, temperature, and plume density changes may be more clearly observed. These effects are lost in black and white film and reproduction. The frames shown in Fig. 3(a) and 3(b) correspond to approximately the same time period in the pulse. The film strip from which the photographs of these figures were taken were run at a framing rate of 25,000 frames/sec. The interframe time therefore corresponds to 40 μsec. Figure 3(a) shows the interaction with alumina when $I = 2 \cdot 10^7$ W/cm^2 ; B, from Eq. (1), is estimated to be $\ll 1$. Figure 3(b) is of copper for the same intensity: B is estimated to be of the order of 1. Note the absence of particulate matter for the copper sample. The comparison between the photographs demonstrates the effect of absorption of the different materials to the laser wavelength for the same intensity.

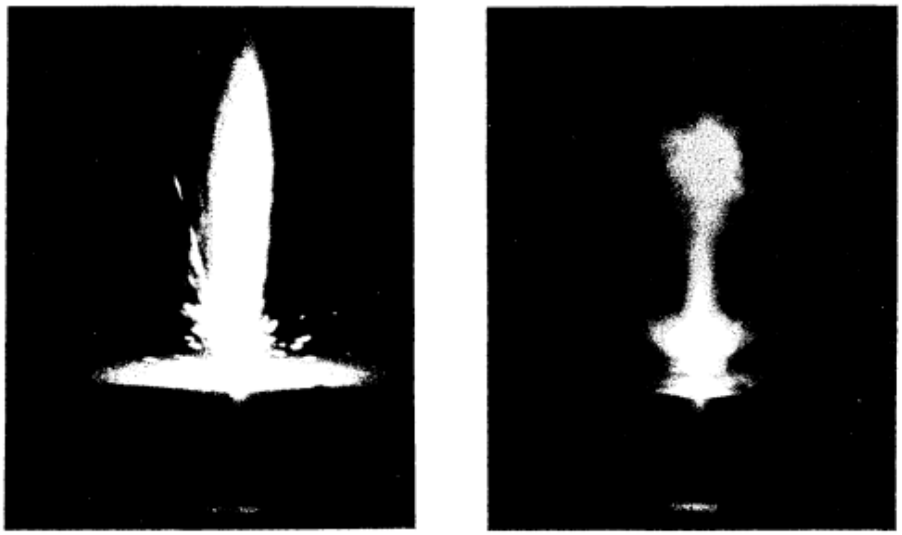

Fig3. *Comparison of explosion for two different B values by changing material constant but same intensity. (a) Al_2O_3; (b) Cu [3].*

This is shown dramatically in Figs. 4(a) and 4(b) for alumina ceramic (830 000 frames/sec). Here the material properties remain constant but the laser intensity is changed from $7.0 \cdot 10^7$ W/cm^2 for the case shown in Fig. 4(a) to $1.3 \cdot 10^7$ W/cm^2 for that of Fig. 4(b). It is clearly seen from the photographs that the amount of particulate matter ejected from the specimen is quite different and that the strength of the explosion in Fig. 4(a) is more energetic.

Volume rxplosive processes may be demonstrated on the examples of 4H-SiC [16, 17] and KCl [18].

In contrast to the formation of surface explosion, three-dimensional periodic structures were obtained in this case. Focused laser irradiation with wavelength 800 *nm* and pulse duration 130 *fs* was used for the irradiation hexagonal silicon carbide 4H-SiC (Fig. 4.7). Sectional area of these structures was ~ 22 μm, the depth of ~ 50 μm. As seen from Fig.4.7(c) we have five stages disordered regions, which are located at a distance from 2 to 4 μm apart vertically [123, 124]. Branches themselves in this case have a thickness from 150 to 300 *nm*. In this case, there are lines in the irradiated nanocavity spherical diameter of from 10 *nm* to 20 *nm*, and irradiated structures have crystallographic symmetry of the initial structure.

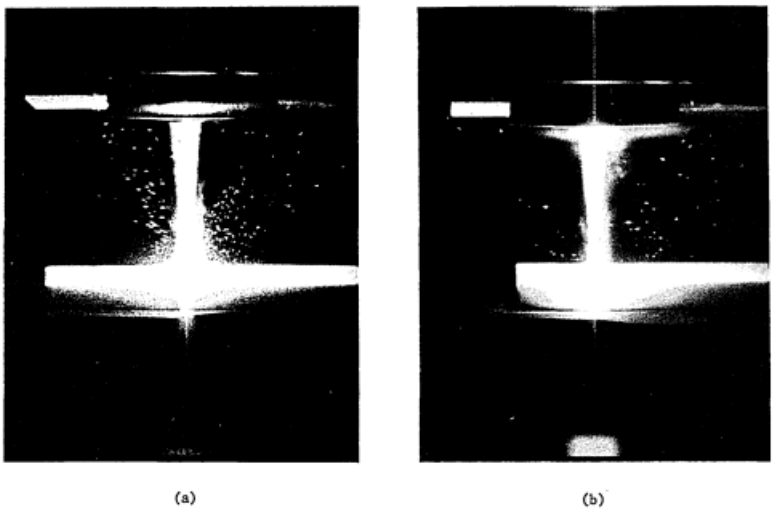

Fig4. *Comparison of strength of explosions for two different B values by changing laser intensity but same material. The object seen above the plume is the focusing lens assembly. (a) I = 7·10^7 W/cm^2; (b) I = 1.3·10^7 W/cm^2 [3].*

We see minimum five stages of destruction cascade on Fig. 5(c) and seven in Fig. 6. However, really the number of diffractive rings may be more as two.

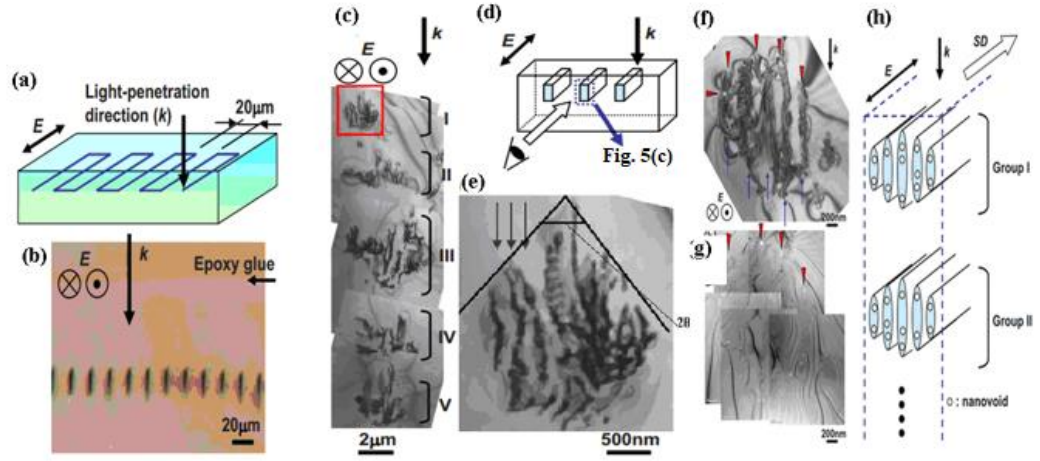

Fig5. *(a) Schematic illustration of the laser irradiated pattern. The light propagation direction (k) and electric field (E) are shown. (b) Optical micrograph of the mechanically thinned sample to show cross sections of laser-irradiated lines (200 nJ/pulse). (c) Bright-field TEM image of the cross section of a line written with pulse energy of 300 nJ/pulse. (d) Schematic illustration of a geometric relationship between the irradiated line and the cross-sectional micrograph. (e) Magnified image of a rectangular area in (c). Laser-modified layers with a spacing of 150 nm are indicated by arrows. (f) Bright-field TEM image of a portion of the cross section of a line written with a pulse energy of 200 nJ/pulse. (g) Zero-loss image of a same area as in (f) with nanovoids appearing as bright areas. Correspondence with (f) is found by noting the arrowheads in both micrographs. (h) Schematic illustrations of the microstructure of a laser modified line. Light-propagation direction (k), electric field (E), and scan direction (SD) are shown. Only two groups (groups I and II) of the laser-modified microstructure are drawn [16, 17].*

In this case diffraction processes may be generated in two stages: 1 – formation of diffraction rings of focused beams [11, 12, 19] and second – formation of diffracting gratings in the time of redistribution of second-order Cherenkov radiation [19].

Two damages region in a crystal with moderately high density of inclusions were received in [18] for potassium chloride *KCl* after irradiation by CO_2-lase pulses (wavelength 10,6 μm, duration of pulse 30 *ns*). The laser was known to be operating in the lowest-order transverse Gaussian mode. There were

several longitudional modes, however, which contributed a time structure to the pulse, periodic at the cavity round-trip time. The phase relationships between the longiotudional modes varied from shot to shot, changing the details of the time structure and causing the peak of the envelope to fluctuate by ±15% [18]. These results are presented in Fig. 6 [18].

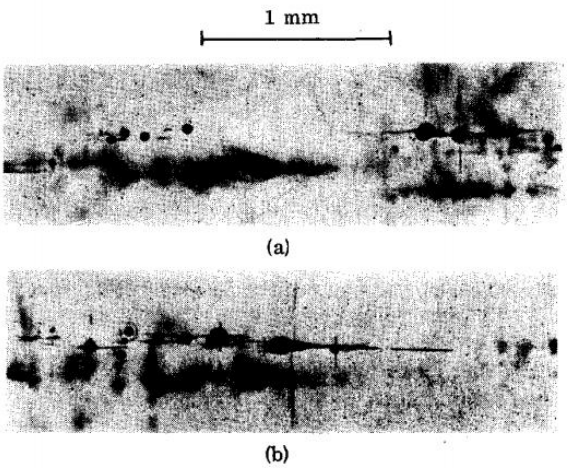

Fig6. *Two damages region in a crystal KCl with moderately high density of inclusions. The round black objects are bubbles. The radiation, incident from left to right, was yust at the intrinsic breakdown threshold. In one case (a) there was damage only at the inclusions. In (b), intrinsic breakdown occurred as evidenced by the pointed bubble. The straight lines represent cleavage [18].*

Successive laser shot (1/sec) were focused into bulk single crystals using a 1–inch focal length "Irtran 2" lens. The breakdown was monitored by observing the visible light from the focal region and by examining the damaged region under the microscope. It was found that most of the crystals suffered some damage even at relatively low power levels. The threshold of this type of damage varied by an order magnitude from one position in the crystal to another. At any particular energy level, damage would occur on the first laser shot or not at all.

Fig. 6(a) shows that spatial inhomogeneities are in fact inclusions [18]. The damage bubbles occur randomly near, not necessarily in, the tiny focal volume. At a well-defined power threshold, an elongated pointed bubble forms, its vertex falling at the focus (Fig. 6(b)). This power level is regarded ass the bulk intrinsic breakdown threshold. Its value is reproducible in crystals from different manufacturers, with inclusions or without. When no inclusion-free samples of a compound were available, the considerations mentioned above were used to determine the dielectric strength [18].

Rough schematic of interactions, and explosive consequences, of laser interactions may be represented according to [22] (Fig. 7)

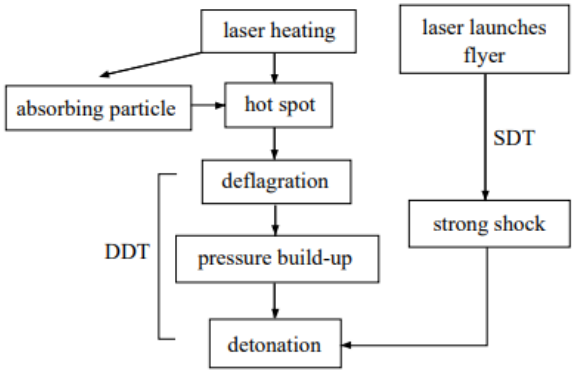

Fig7. *Schematic of interactions, and explosive consequences, of laser interactions [32].*

3. MODELING AND DISCUSSIONS

3.1. Some remarks

As can be seen from Fig. 3 - Fig. 6 jet of substance ejected outwards has a directional direction and resembles a bomb explosion in shape. However, the mechanisms here are different. If detonation and

an explosive wave are used in a bomb explosion, then in the case of a laser, physico-chemical processes often play a major role.

As can be seen from Fig. 3 - Fig. 6 jet of substance ejected outwards has a directional direction and resembles a bomb explosion in shape. However, the mechanisms here are different. If detonation and an explosive wave are usiung in a bomb explosion, then in the case of a laser, physico-chemical processes often play a major role.

Obtaining frames corresponding to Fig. 2, this is a rather problematic task, since there are a number of processes that precede detonation in the classical sense of the word.

Therefore, forms of Fig. 3 and Fig. 4 may be explaining with hep catastrophe theory with using elliptic, paraboloic and hyprbolic umbiliqus.

When creating a classical explosion, the geometry of the experiment plays a big role. Thus, when designing a thermonuclear bomb, the geometry of the detonator and the working substance is of great importance [31, 35, 36]. Thus, in A. Sakharov's heterostructural schemes, the layers of the detonator border the layers of the working substance, with a maximum explosion energy of 20 megatons. In spherical Ulam-Teller scheme detonator is placing in center of bomb, working substance is plased in other volume. In thi case we have unlimited maximum explosion energy. As example we represent scheme of undewater explosing device.

3.2. Ballard model

When irradiating a metallic target with a laser pulse, one can reach a fluence of about 10 GW/cm2. A high pressure plasma is then formed at the surface of the target (Fig. 8 a)) [8]. Some previous studies have shown that the pressure is higher when a tranparent overlay is put at the surface of the target in such a way that the plasma is formed at the interface of the target and the transparent overlay. This configuration is called confined geometry [8].

We are going to show that it is possible to evaluate the resulting pressure by mean of a very simple model (Fig. 8 b)). We suppose that the laser irradiation on the surface is equivalent to a constant intensity Φ, applied while a duration τ. During irradiation, the instantaneous energy on target surface is then at. We assume that a part $1-\alpha$ of this energy is devoted to ionize the plasma. The rest $\alpha\Phi t$ is stocked in the plasma, assumed to be a perfect gas, as thermal and mechanical energy.

$$\alpha\Phi t = \frac{3}{2}n(t)kT(t) + P(t)[L_t(t) + L_0(t)], \tag{2}$$

$$\alpha\Phi t = \frac{5}{2}P(t)[L_t(t) + L_0(t)], \tag{3}$$

The transparent overlay is supposed to be an elastic solid and the target an elasticplastic solid. Under these hypothesis, one can show that the resulting pressure is [8]:

$$P(t) = \frac{(c_e-c_p)\rho_0 c_0}{2c_0(\rho_0 c_0+\rho c_p)}\left(1+\frac{\lambda}{2\mu}\right)\sigma_Y + \sqrt{\left[\frac{(c_e-c_p)\rho_0 c_0}{2c_0(\rho_0 c_0+\rho c_p)}\left(1+\frac{\lambda}{2\mu}\right)\sigma_Y\right]^2 + \frac{2}{5}\frac{\rho\rho_0 c_0 c_p \alpha\Phi}{\rho_0 c_0+\rho c_p}}, \tag{4}$$

were: ρ_0 is the specific mass of the transparent overlay; c_0 – the speed of elastic longitudinal waves in the transparent overlay; ρ – the specific mass of the target; λ and μ – the elastic Lame's constants of the target σ_Y, the uniaxial elastic limit of the target; c_e and c_p – the speeds of elastic and plastic longitudinal waves in the target.

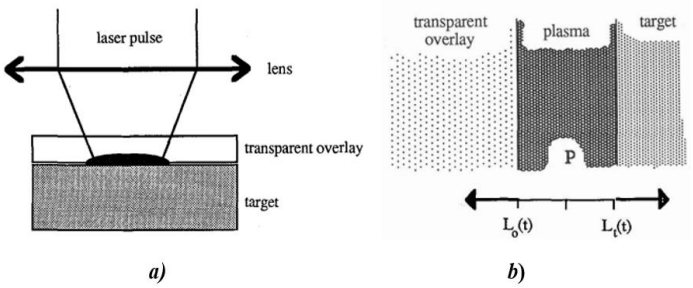

Fig8. *a) conditions of irradiation; b) schema of modelling [8].*

We have the relations [8]:

$$c_e = \sqrt{\frac{\lambda+2\mu}{\rho}};\ c_p = \sqrt{\frac{\lambda+{}^{2\mu}/_{3}}{\rho}}. \quad (5)$$

This result has been compared with piezo-electric quartz pressure measurements. It appears that the value of the parameter a seems to be independant of the intensity and the duration of the laser pulse (at least in the range of 1 to 100 GW/cm2 and 3 to 30 ns). In all cases, α is about 0.25 [8].

3.3. Cumulation. Classical case

Cumulation is the concentration of the action of the explosion in a certain direction. It is achieved by the form of charges of an explosive substance — the so-called by a cumulative notch in the opposite part of the charge from the detonator (on the end of the cartridge – an end, or on its base –a longitudinal cumulative notch). When the explosion is initiaing, the products of the chemical reaction form a directed flow with high-speed (10-15 km/s) cumulative jet is formed, which ensures its high penetrating power. In mining, the cumulative effect is using for crushing oversize, perforating wells [31].

Let us consider in more detail the model of a cumulative underwater explosion, in which the shock wave can spread for 20 km (Fig. 9) [31]

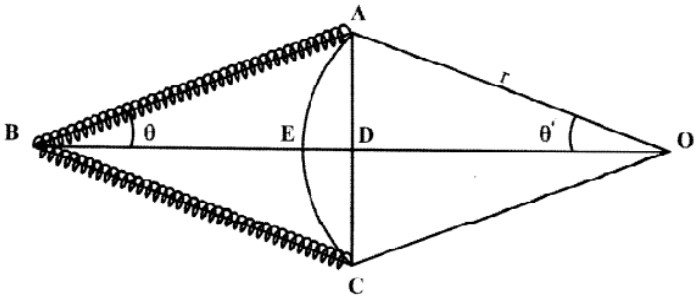

Fig9. *Schema of a cumulative underwater explosion [31].*

Triangle ABC shows a longitudinal section of a cone with angle Θ at vertex B. The side surface of the cone (sections BA and BC in the drawing) is lined with hexogenstrands wound into a spiral. There are n=36 such spirals in total, and they are located along azimuth at equal angular intervals, in this case ΔΘ=10°. Angle at top of the cone Θ, the pitch and radius of the spiral winding are chosen such that the projection the velocity of propagation of the blast wave to the height of the cone was equal to the velocity propagation of sound in water. Then the sound wave from breaking any point spiral, will come simultaneously to the entire base of the cone, in projection to points A, D and C. If the spirals are wound with variable pitch and winding radius, then it is possible form a spherical concave blast wave front, the cross section of which is the drawing is shown by points A, E, C. Such a spherically converging sound (percussive) the wave will focus at point O, located at a radius r from the cone. At an angle convergence Θ' much smaller than Θ, the focusing radius will be much larger than cone height [31].

Selection of basic parameters [31]:

1. Explosion dynamics [31]. .

For water, the compressibility coefficient is $k_{H_2O} = 5 \cdot 10^{-5}$ atm-1. For pressures less than 103 atm, the water density in the shock wave differs little fromdensity under normal conditions and the speed of the shock wave is approximately equal to speed of sound: v_{H_2O}≈1.5 km/s.

2. Choice of angle solution at the top of the cone [31].

Since the speed of the detonation wave in hexogen is v_{dw}= 8.36 km/s, [5], significantly exceeds the speed of sound in water v_{H_2O}≈1.5 km/s, then to create plane front of the shock (sound) wave, it is necessary to choose the opening angle of the cone equal to:

$$\Theta_{pf1} = \arccos\frac{v_{H_2O}}{v_{dw}} = 0.18. \quad (6)$$

Corresponding angle between detonation wave velocity and sound velocity in this case it is equal to: Θ_{pf1}=80°.

Next, choose Θ_{pf2}=45°.

3. Formation of a flat front of a sound wave by a cone with an angle at the top,

equal to: Θ_{pf2}=45° [31].

To obtain such an angle between the direction of the blast wave and the speed sound in water, it is necessary to slow down the speed of propagation of the blast wave. This can be done if you "lay out" the side surface of the cone with hexagon strands wound into a spiral. Let there be n=36 such threads in total, that is, in azimuth they will be evenly spaced every 10 degrees.

The process of slowing down the explosive wave in the spiral is purely geometric: the actual detonation wave propagates along the spiral with a velocity v_{dw} .=8.36 km/s, the speed of propagation of the explosive wave along the axis of the spiral is less, it is equal to:

$$v_{ew} = \left({}^{h_s}/_{2\pi r_0}\right) v_{dw}, \tag{7}$$

where h_s is the winding pitch of the spiral, r_0 is the radius of the spiral.

Let's choose the spiral winding radius equal to: r_0=25 cm. Then the diameter of such a hexogen helix is equal to ds = 50 cm. To make the angle between the blast wave velocity and the speed of the sound wave was: Θ_{pf2}=45°, blast wave speed, the velocity of propagation of the detonation wave along the axis of the helix should be v_{ew}=2.14 km/s and the pitch of the spiral should be equal to:

$$h_s = \left({}^{2\pi r_0}/_{v_{dw}}\right) v_{ew}. \tag{8}$$

Let the diameter of each hexogen filament be dhf = 1 cm. The length of the generatrix of the cone is approximately one and a half times greater than half the diameter of the cone, which we chose equal to: Dcone =150 m,

$$l_{gc} = \frac{D_{cone}}{2\cos 45^\circ} = 107\ m. \tag{9}$$

Along the generatrix fits $n = {}^{l_{gc}}/_{h_s}$ = 267 turns of the spiral, so that its total length, with the length of the turn 2πr0=1.57 m, will be: l_s=420 m.

The volume of each spiral, with a hexogen filament diameter equal to: df =1 cm, will be equals:

$$V_s = \left({}^{\pi d_f^2}/_{4}\right) l_s = 3.3 \cdot 10^{-2} m^3. \tag{10}$$

The mass of one hexogen filament will be equal to: $M_f = \rho_h \cdot V_s$ = 60 kg, the total mass of hexogen in n = 36 spirals arranged along the lateral surface of the cone will be equal to: $M_t = M_f \cdot n$ = 2.16 tons.

The energy release of RDX during the explosion is, [5], 1.37 kcal/kg or 5.75 GJ/ton. Such the amount of explosive located on the side surface of the cone, seems acceptable.

4. Spatial and temporal duration of the shock wave front [31].

The time duration of the front of such a wave will be short, of the order τfr =πr0/v_{dw} ≈0.1 ms. This is due to the fact that various sections of the spiral explode sequentially, and the projection of the blast wave velocity on the height of the triangle as times equal to the speed of sound. From two points located on the diameter, on the same distance from the focus, a blast wave propagating along the height triangle, will come with a delay τfr =πr0/v_{dw} ≈ 0.1 ms.

Considering the value τfr as a half of the period corresponding to this duration sound wave, we find that the period of the wave T0 is equal to: T0= 4τfr =0.4 ms. Frequency sound wave in this case is equal to: fs = 2.5 kHz and the distance at which the sound is frequency will reduce its intensity by a factor of 10, is about 100 km[6].

This frequency of the sound wave fs = 2.5 kHz corresponds to the wavelength: $\lambda_s = {}^{v_s}/_{f_s} = 0.6\ m$.

5. Propagation of a plane front of a sound wave by a cone with an angle at top, equal to: Θ_{pf2}=45° [31].

Consider the propagation of a sound wave formed by a flat front. The diffraction limit, the minimum angle of divergence of such a flat front will be equal to:

$$\Theta_{expl}={}^{\lambda_s}\!/_{D_{cone}}. \quad (11)$$

and the size of the area occupied by the sound wave will be equal to:

$$\Delta y = \Theta_{expl} \cdot F, \quad (12)$$

where F is the distance to the observation point, in our case F=20 km.

Substituting the numbers in the formula (12): λ_s = 0.6 m, D_{cone}=150 m, $\Delta y = 80\ m$.

The explosion energy of a hexogen spiral will be uniformly distributed over a solid angle of 4π, and only a corresponding small part of the entire explosion energy will be concentrated in the spatial minimum angle of divergence.

6. Pressure at the front of a sound wave [31].

Let us estimate the pressure at the front of the sound wave based on the following considerations.

The total energy release of the explosion is:

$$\Delta Q = M_t \cdot 5.75 = 12 \text{ GJ}. \quad (13)$$

With a pulse duration equal to τfr = 0.1 ms, the explosion power will be equal to:

$$W = {}^{\Delta Q}\!/_{2\tau_{fr}} = 60TW. \quad (14)$$

Thus, the intensity of the sound wave at the front can be estimated as

$$I = {}^{I}\!/_{4\pi F^2} = 25\ {}^{kW}\!/_{m^2}. \quad (15)$$

The pressure in the sound wave will be

$$P = \left(I \cdot \rho_{H_2O} \cdot v_s\right)^{1/2} = 2 \cdot 10^5 Pascal = 2\ atm. \quad (16)$$

Such a pressure, at a distance F=20 km from the point of explosion, is of practical interest for a number of applications.

7. Formation of a concave spherical front of a sound wave by a cone with an angleat the top equal to Θ_{pf2}=45° [31].

If in a point explosion only a convex spherical front can be obtained, then in the explosion of a cone, the side surface of which is lined with hexogen strands of spiral shape, both flat and concave spherical front can be obtained.

To obtain a flat front, it is necessary that the propagation velocity of the explosive wave was constant and exceeded the speed of sound propagation in water, formula (8). To get a concave spherical front, you need to create variable, increasing as the explosion propagates, the speed of propagation of the blast wave.

Let us find the conditions under which the time of arrival of the front of the sound wave at the focus point O will be the same when any point on the spiral breaks, that is, any a point lying on the segment AB or BC on the lateral surface of the cone.

Let us designate the segment BO - from the top of the cone to the focus of the spherical front as l0. We denoted the distance AB by the value lb, then:

$$l_0 = l_b \cos\Theta + \left(r^2 + l_b^2 \sin^2\Theta\right)^{1/2}, \quad (17)$$

let us denote the time during which the sound wave travels the distance l_0 as t_0, so that

$$t_0 = {}^{l_0}\!/_{v_s}. \quad (18)$$

For the same time t0, the sound wave must reach the point O from any point located on the spiral. Let's denote the distance from point B - the top of the cone, to this certain point as x. Then the distance from this point x to the point O - the center of the sphere - is equal to r1:

$$r_1^2 = (x\sin\Theta)^2 + (l_0 - x\cos\Theta)^2. \quad (19)$$

When the focus point O is removed to a distance much greater than the height or side of the cone, the concave spherical wave front will be almost flat, thenis the velocity of propagation of the explosive wave $v(x)$ along the lateral surface of the cone will be almost equal to v_s. Imagine $v(x) = v_s + \delta v$, where $\ll v_s$. Let us find δV from the relation

$$v(x)\cos\Theta = v_s\cos\Theta + \delta v\cos\Theta. \quad (20)$$

For the time corresponding to the passage of the blast wave of the side surface of the cone tb about $t_{ss} = {}^{l_0}/_{v_s}$, the difference between $v(x)\cos\Theta t_{ss}$ and $v_s\cos\Theta$, equal to $\delta v\cos\Theta t_{ss}$, is equal to a - the height of the chord:

$$a = \left[r^2 - \left(r^2 - l_b^2\sin^2\Theta\right)\right]^{1/2}, \quad (21)$$

where:

$$\delta v = {\left[r^2 - \left(r^2 - l_b^2\sin^2\Theta\right)\right]^{1/2}}/{\cos\Theta \cdot t_{ss}}. \quad (22)$$

The dependence of the velocity of propagation of the explosive wave $v_x(x)$ is weak and you can choose, for example, $\delta v_1 = {\delta v \cdot x}/{l_b}$, so that at $x = l_b$ the addition to the speed δv_1 is equal to δv.

If the speed of the blast wave $v_s(x)$ will change as it propagates along the lateral surface of the cone in accordance with the law, $(x) = v_s + \delta v$, $\delta v_1 = {\delta v \cdot x}/{l_b}$, $\delta v = {\left[r^2 - \left(r^2 - l_b^2\sin^2\Theta\right)\right]^{1/2}}/{\cos\Theta \cdot t_{ss}}$ then the arrival time of the soundwave (blast wave front) to point O will be the same for all points located on the lateral surface of the cone.

It is possible to change the speed of propagation of the explosive wave along the lateral surface of the cone by the step and radius of the spiral winding in accordance with formula (8).

8. Focal length [31].

If the speed of propagation of a sound wave along the height of the cone with the opening angle at the top, equal to Θ_{pf2}=45°, will be less than the speed of the blast wave, propagating along the axis of the spiral along the lateral surface of the cone, then a concave front of the sound wave is formed at the base of the cone.

Let's make a cross section of the cone, we get a triangle. We denote by points A and C the points lying at the base of the triangle, and by point B - its apex. Point D let lies at the intersection of the base of the triangle with its height, then point E, lying on the same circle of radius r as points A and C, is inside the triangle ABC. Let us denote by the value a the distance ED - the difference between the flat and concave front on the axis, the value b - the distance AD - half the width the base of the cone. By the point O we denote the center of the circle of radius r passing through the points AED, the angle AOE is denoted by the value Θ'.

Then: (r-a)/r=sinΘ', b/r=cosΘ', we write the identity: sin2Θ'+cos2Θ'=1, in the form:

$$\frac{(r-a)^2+b^2}{r^2} = 1, \quad (23)$$

where we find the radius of the circle:

$$r = \frac{a^2+b^2}{2a}, \quad (24)$$

and, given that a << b, we get:

$$r \approx \frac{b^2}{2a}. \quad (25)$$

So, if we want to focus the blast wave at a distance of r =20 km, for $= {}^{D_{cone}}/_{2} = 75\ m,$, we will have to withstand: $a = \frac{b^2}{2r} \approx 0.3\ m.$

The pressure at the focus of such a converging sound wave will at least notless than the pressure at the front of a plane sound wave: P >2 atm.

The time during which the blast wave propagates from the cone to a distance r =20 km will be slightly more than 13 seconds [31].

3.4. Laser-induced optical breakdiown as volume explosion

Now we represent cascade model of laser-induced optical breakdiown. This cascade is including next stages: focusing of laser radiation, diffraction stratification, surface Cherenkov radiatoon, interference of shortwave Cherenkof radiation and optical breakdown in maximum of its interferogram [11, 12, 19]. Roughly speaking is "laser" variant if volum cumulation.

It should be noted that a possible and symmetrical laser-induced breakdown (explosion) in the form of a star [34].

The determination the concentration of scattering centers must be determined with conditions of proper experiment. It is determined by the conditions of observation the proper phenomena.

Next step of determination the density of energy in our cascade is condition of diffraction stratification. This condition may be determined with help of sizes the diffraction rings. We can estimate density of energy in plane of creation the diffraction stratification for *n*=5.

For bond of focusing and Cherenkov angles the synthesized A. Bohr-I. Golub formula is using [19]

$$\theta_{ch} + \alpha_{ir} = {}^{\pi}/_{2} \text{ or } \theta_{ch} = {}^{\pi}/_{2} - \alpha_{ir}, \quad (26)$$

Where θ_{ch}– Cherenkov angle; α_{ir}– angle between tangent line and direction of laser beam.

Angle α_{ir} was determined from next formula [11, 12, 19]

$$tan\alpha_{ir} = {}^{d_b}\Big/_{l_f}, \quad (27)$$

where d_b – diameter of laser beam, (7 *mm*), l_f – length of focusing or self-focusing. In our case α_{ir} is angle of focusing or self-focusing.

This formula is approximate for average angle α_{ir}.

The estimation of sizes the cascade of volume destructions of 4H-SiC [16, 17] may be explains in next way [11, 12, 19]. The sizes (diameters) of proper stages d_{nir} of cascade are proportionally to corresponding diffraction diameters d_{ndif}

$$d_{nir} = k\, d_{ndif}, \quad (28)$$

where *k* is the proportionality constant.

The diffraction diameters d_{ndif} may be determined with help condition of diffraction-pattern lobes (modified Rayleygh ratio)

$$d_{ndif} = n\lambda. \quad (29)$$

The estimations of first five diffraction diameters d_{ndif} for λ = 800 *nm* were represented in [7, 8].

The distance between diffraction spots and proper moving foci may be determined with help next formula [11, 12, 19]

$$l_{nf} = \frac{d_{ndif}}{2\tan {}^{\varphi}/_{2}}. \quad (30)$$

These distances for φ_1 = 20º and φ_2 = 30º were represented in [7]. In general case the angle φ is depended from homogeneity of irradiated matter or intensity of irradiation.

Therefore, for 4H-SiC (Fig. 5) we give 5 stages, for KCl – 7 stages (Fig. 6).

Qualitative explanation of development of cascade the destructions may be next. The focus of each diffraction zone (spot) is the founder proper shock optical breakdown. However, foci with more high number may placed in the "zone" of influence of previous foci. Therefore, only first stage for 4H-SiC (Fig. 5(c)) is represented pure shock mechanism (Mach cone). Mach cones are characterized the second and third stages of 4H-SiC (Fig. 5(c)). However, its maximums are displacing from center. It may be result if interaction second and third shock waves with previous shock waves: first – for second wave and first and second for third wave. The chock mechanism of destruction certifies a linear direction of optical breakdown. This direction is parallel to direction of shock wave and radiated spectrum is continuum as for Cherenkov radiation and as for observed laser-induced filaments in water and air [11, 12]. Thus, basic creator of optical breakdown traces is secondary Cherenkov radiation and shock waves. This radiation is absorbed more effectively as laser radiation and therefore the creation of optical breakdown traces is more effectively as for beginning laser radiation. Cherenkov radiation is laid in self-absorption range of 4H-*SiC*, but 800 *nm* radiation – in intrinsic range. For the testing of this hypothesis, we must measure the spectrum of secondary radiation. In this case, we can use physical-chemical cascade model of excitation the proper chemical bonds of irradiated matter in the regime of saturation the excitation [16, 17].

The conclusion about diffractive stratification of focused radiation may be certified by corresponding experimental data of 4H-SiC(Fig. 5(c)).

We can rough estimate basic peculiarities of energy distribution in Mach cone may be used next formula [12, 19]

$$E_{1ob} = \frac{\pi^2}{4}\left(\sum_{i=1}^{5} n_{iav}^2\, l_{iav}\right) r^2 N_{aSiC} E_{Zth}, \tag{31}$$

where n_{iav}– average visible number of filaments in proper group of cascade, l_{iav}=1000 *nm* – average length of filaments in proper group of cascade, r = 10 *nm* – average radius of filament, N_a – atom density of 4H-*SiC*. For 4H-*SiC* $N_{aSiC} = 9.4 \cdot 10^{21} cm^{-3}$.

For further estimation we use next approximation $n_{1av} = n_{2av} = n_{3av} = n_{4av} = n_{5av} = 100$ [12, 19].

Energy, which is necessary for the optical breakdown our nanotubes may be determined in next way. Zeitz threshold energy for 4H-*SiC* is equaled $E_{Zth} \sim 25\ eV$ [12, 19]. Let this value is corresponded to energy of optical breakdown. Therefore, summary energy E_{1ob} is equaling

$$E_{1ob} = N_{asnt} \cdot E_{Zth} = 23.2\ nJ. \tag{32}$$

This value is equaled of ~ 8% from pulse energy or ~ 30% from the effective absorbed energy of pulse. In this case we have more high efficiency of transformation initial radiation to "irreversible" part of Cherenkov radiation. It is result of more intensive excitation comparatively with classical methods of receiving the Cherenkov radiation. In this case we have pure photochemical processes. The experimental data for intrinsic absorption [11, 12] show that for short pulse regime of irradiation (femtosecond regime) basic processes of destruction the fused silica and calcium fluoride are photochemical (multiphoton absorption in the regime of saturation the excitation). Nevertheless, basic peculiarity of experimental data of Fig. 5 [16, 17] is transformation the initial laser radiation (wavelength 800 *nm*) to continuum Cherenkov radiation. From length of optical breakdown in 4H-SiC we can determine average absorption index of Cherenkov radiation. It is ~ 10^4 cm^{-1}. This value is corresponded to violet-blue range of absorption spectrum of 4H-*SiC* [12].

Concept of diffractive stratification allows explaining the surface character of Cherenkov radiation. This radiation is generating in the region of corresponding focused diffractive ring [12, 19].

In our case, 4H-SiC (Fig. 5(h)) sizes of our nanovoids are equaled 15 – 20 *nm*. Therefore, we must change "sound" mechanism of creation cavitations bubbles on electromagnetic. Roughly speaking, this problem was resolved with help change speed of sound or speed of light.

The sizes of nanovoids 4H-SiC (Fig. 5(h)) may be determined with help modified Rayleygh model [1, 11, 12, 19] and its form – the help methods of continuum mechanics [1-5] in next way.

Nanovoids may be representing as results of the laser-induced laser-induce breakdown and creation of cavitations bubbles (Fig. 5(h)) too. The light pressure may be determined with help of next formula [12, 19]

$$p_0 = \frac{E_{ir}}{\tau_i c S}, \tag{33}$$

where E – energy of irradiation, τ_i – pulse duration, S – area of irradiation zone, c – speed of light. For circle symmetry

$$S = \pi r^2, \tag{34}$$

where r – radius of laser spot.

For the estimations of maximal radius of nanovoids we must use modified Rayleygh formula [11, 12, 19]

$$R_{max} = \frac{2R}{0.915r}\sqrt{\frac{E_{ir}}{\pi\tau_{ir}cE}}, \tag{35}$$

where T_c – the time of creation the nanovoid (bubble), R is radius of nanovoid, r – radius of irradiated zone, E – Young module, E_{ir}– energy of one pulse. τ_{ir} – duration of pulse [11, 12, 19].

If we substitute r = 250 *nm*, R = 10 *nm*, E = 600 *GPa* [11, 12, 19], E_{ir}=300 *nJ*, τ_{ir} = 130 *ps*, c=3·10^8 *m/s*, than have R_{max}=11 *nm*.

The speed of shock waves for femtosecond regime of irradiation is less as speed of sound. However, we have two speeds of sound in elastic body: longitudinal v_{ls} and transversal v_{ts} [7-10, 15]. Its values are determined with next formulas

$$v_{ls} = \sqrt{\frac{E(1-\nu)}{\rho_0(1+\nu)(1-2\nu)}}, \text{ and } v_{ts} = \sqrt{\frac{E}{\rho_0(1+\nu)}}, \tag{36}$$

where ν – Poisson's ratio [11, 12, 19]. The ratio between of these two speeds is equaled

$$\alpha = \frac{v_{ts}}{v_{ls}} = \sqrt{\frac{(1-2\nu)}{2(1-\nu)}}. \tag{37}$$

However, this ratio must be true for shock waves too. Therefore, for silicon carbide for ν = 0,45 [11, 12, 19] α = 0,33. Roughly speaking last ratio is determined the step of ellipsoidal forms of our nanovoids (Fig. 5 (h)).

In [11, 12, 19] allow estimating maximal longitudinal and transversal $R_{max,i}, i \in (l,t)$. These values are 6 *nm* and 19 *nm* properly.

In this case, we represented 4H-SiC as isotropic plastic body. For real picture, we must represent hexagonal structure. However, for the qualitative explanation of experimental data of Fig. 6 this modified Rayleygh model allow explaining and estimating the sizes and forms of receiving nanovoids [12, 19].

Laser-induced shock processes have specific peculiarities. In general case we have electromagnetic and acoustic shock processes [19]. Formally, these processes have similar nature.

Speed of electromagnetic shock processes (speed of polarization the media in the result of corresponding interaction) must be more as phase speed of light in media. In this case, phase speed of light in media has next physical nature: it is speeding of collectivization the electromagnetic oscillations for proper frequency. Roughly speaking it is electromagnetic characteristic of media, which is corresponded to its electron and ion subsystems. Example of this type process is Cherenkov radiation. In this case, we have radiated reaction of media on heterogeneity excitation of media in shock regimes of interactions.

Speed of acoustic shock processes (speed of motion proper object in media) must more as speed of sound in media [19]. However, speed of sound is media is average heat speed of media, which is connecting with atomic structure of media. Examples of these processes are: flight of airplaine or rocket in with supersonic speed; various explosions. Roughly speaking, explosions may be characterize as chemical process with speed more as sound speed in media. Mach number is characterize in this case the macroscopic "detonation" of corresponding process.

Both processes (electromagnetic and acoustic) are characterized by Much cone, which is created by proper vectors of speed processes or object and speed characteristic of media (polarization or sound) [19]. Laser-induced shock processes may be representing as analogous to acoustic explosions. But this process is realized with electromagnetic speed. In this case we must have "electromagnetic" explosion as Cherenkov radiation [19].

In whole the nonequilibrium and irreversible shock, processes may be having electromagnetic and acoustic nature [19].

Now we used physical-chemical method of estimation for the modeling experimental data for *KCl* (Fig. 6). Density of atoms of KCl equal $3.1 \cdot 10^{22} cm^{-3}$, Zeits energy for KCl has value ~ 30 *eV* [19].

Results of modeling are representing in [12, 19].

We used next approximations. Photography of Fig. 4 gives a blurry image compared to the bright-field TEM image of Fig. 5. Therefore, we can't see the microstructure of optical breakdown. And we use rough average approximations for diameter $d_{average}$ and length l of cascade laser-induced optical breakdown of Fig. 6 [7, 8]. Volume of cascade was determined as cylinder volume.

Fig. 6 is similar to Fig. 5 c). However, regimes of irradiation of Fig. 4 are similar to mode TEM_{01}. Therefore, we have two channels of generation the cascade of laser-induced optical breakdown.

The distances between bubbles of Fig. 6 (b) are more as between regions of destruction of Fig. 5(c). However, conditions of focusing the radiation in these both cases are equivalence. Therefore, the distances between neighboring bubbles l_2 *KCl* and neighboring regions of destruction l_1 of 4H-SiC [12, 19] are connecting by next formula

$$l_2 = \frac{d_{ndif2}\tan\left(\varphi_1/_2\right)}{d_{ndif1}\tan\left(\varphi_2/_2\right)} l_1 = \frac{\lambda_2\tan\left(\varphi_1/_2\right)}{\lambda_1\tan\left(\varphi_2/_2\right)} l_1. \quad (38)$$

In whole, the correlation of this distasnces is depended from wavelength of irradiation and focusing angles, including intensity of irradiation. Which is determined the step of homogeneity of irradiated matter. If we substitute in formula (38) $\lambda_2 = 10.6\mu m$ and $\lambda_1 = 0.8\mu m$ and $\varphi_1 = \varphi_2$ then we'll receive

$$l_2 = 13.25 l_1. \quad (38\ a)$$

Energy characteristics we select from references in [18]. Therefore, we select value 2 *J*/*pulse* from [12, 19]. In this case we have effective using energy. Methods of estimations of energy characteristics for *KCl* are rougher as for 4H-*SiC*. But we must suppose that focused laser irradiation has diffraction stratification, generation of Cherenkov radiation and interference of this Cherenkov radiation. For KCL 5-7 stages of cascade optical breakdown we see. Sources of Cherenkov radiation id diffraction stratified cones.

If this scenario is true, we have as for 4H-SiC effective transformation the energy of laser radiation to cascade of laser-induced breakdown for *KCl* too. This value is 11,6 – 17,4 percents [12, 19].

We can estimate sizes and forms of possible nanovoids for potassium chloride too. Let's take the ratio of the radius of the irradiation zone to the radius of the nanowire as 50. The energy of irradiation is 2 *J*. The duration of irradiation is 50 *ns*. Young's modulus 29.67 *GPa*, Poisson's ratio 0.216.

After substitution, these data to formula (35) we have $R_{maxKCl} = 62.5nm$. Ellipticity of *KCl* nanovoids may be determined from (37) $\alpha_{KCl} = 0.6$.

Let us now estimate the maximum bubble radii for the acoustic case. For this, in formula (35), you need to change the speed of light to the speed of sound (35 a).

$$R_{max}^{ac} = \frac{2R}{0.915r}\sqrt{\frac{E_{ir}}{\pi\tau_{ir}c_s E}}, \quad (35\ a)$$

where c_s is speed of sound.

As a result, we get $R_{maxSiC}^{ac} = 1.7\mu m$ and $R_{maxKCl}^{ac} = 28\mu m$. The shape of the voids does not change, they just increase in size by 2-3 orders of magnitude.

If we take the ratio of the acoustic formula (35 a) and the optical formula (35), then for the same irradiation modes we have the ratio [19]

$$\frac{R_{max}^{ac}}{R_{max}} = \sqrt{\frac{c}{c_s}}. \quad (39)$$

However, a comparison with the experimental results 4H-SiC [16, 17] shows those electromagnetic rather than acoustic processes play the main role in the formation of nanovoids. This is explaining by the fact that in this case a chain of close-range coherent processes of transformation of both optical radiation into the excitation of the medium and the corresponding relaxation of the medium is implemented, in other words, there is a chain of interconnected coherent transformations.

Experimental results on optical breakdown confirm the fact that optical breakdown takes place only in the near-surface region and in the short-wavelength region of Cherenkov radiation. It would also be

interesting to investigate the long-wavelength part of Cherenkov radiation. It is quite possible that even at greater depths (from several millimeters to several centimeters) phase transformations of the irradiated material occur. Roughly speaking, these depths are determined by the absorption coefficients of the corresponding radiation. In addition, the regions of different diffraction circles may overlap. In this case, roughly speaking, we can consider an optical breakdown as a variant of a diffraction volume cumulative explosion. At the same time, the conditions of cumulation are created by the conditions of irradiation.

Experimental data for liquid and gases are corresponding to acoustic case and therefore, we can use the Rayleygh and its modified hydrodynamical models for its explanation [12, 19].

4. Conclusion

1. Main concepts of modeling the laser-induced cavity in Nonlinear and Relaxes Optics are observed.
2. Short review of corresponding experimental data is represented.
3. Short analysis of Rayleygh theory of cavitation and its extensions (Rayleigh–Plesset, Gilmore; and Keller–Miksis models) are discussed.
4. Necessary of transition to chain methods of modeling the shock processes of Nonlinear and Relaxed Optical processes as including of prehistory the cavitation is formulating.
5. Cascade model as variant of this prehistory is analysed.
6. The difference between acoustic and electromagnetic shock processes shown on the example the generation laser-induced nanovoids in silicon carbide and potassium chloride.
7. Comparative analysis of other properties of acoustic and electromagnetic chock processes is representing too.

References

[1] Rayleygh (J. W. Strutt) (1917) On the pressure developed in a Liquid during the Collapse of a Spherical Cavity. The London, Edinburgh and Dublin Philosophical Magazine and Journal of Science. Vol. 34, 94-98.

[2] Taylor G. I. (1950) The formation of a blast wave by a very intense explosion. II. The atomic explosion of 1945. Proc. Roy. Soc. A. Vol. 201, 175-186.

[3] Gagliano F. P., Paek U. C. (1974) Observation of laser-induced explosion of solid materials and correlation with theory. Applied Optics. Vol. 13, Is. 2, 274-279.

[4] Detonation. https://en.wikipedia.org/wiki/Detonation

[5] Cavitation. https://www.britannica.com/science/cavitation

[6] Trokhimchuck P. P. (2018) Continuum mechanics. Vezha-Print, Lutsk (in Ukrainian)

[7] Chaban V. V., Pal S., Prezhdo O. V. (2016) Laser-induced explosion of nitrated carbon nanotubes: non-adiabatic and reactive molecular dynamics simulation. J. Am. Chem. Soc Vo. 138, Is.49: 15927-15934.

[8] Ballard P., Fournier J., Fabro R., Frelat J. (1991) Residual stresses induced by laser shock. Journal de Physique IV, Colloque C3, Suppl. au Journal de Physique III, C3-487 – C3-494.

[9] Sano Yuji; Akita Koichi; Sano Tomokazu (2020). A Mechanism for Inducing Compressive Residual Stresses on a Surface by Laser Peening without Coating. Metals. Vol. 10, Is. 6, 816–827.

[10] Wang X., Liu R., He Y., Fu Y., Wang J., Li A., Guo X., Wang M., Guo W., Zhang T., Shu Q., Yao Y. (2022) Determination of detonation characteristics by laser-induced plasma spectra and micro-explosion dynamics. Optics Express. Vol. 30, Is.4, 4718-4736.

[11] Trokhimchuck P. P. (2020) Relaxed Optics: Modeling and Discussions. Lambert Academic Publishing, Saarbrukken

[12] Trokhimchuck P. P. (2022) Relaxed Optics: Modeling and Discussions 2. Lambert Academic Publishing, Saarbrukken-Cisinau; Trokhimchuck P. P. (2022) Relaxed Optics: Modeling and Discussions 2. AkiNik, New Dehly

[13] Trokhimchuck P. P. (2020) In: Laser-induced optical breakdown of matter: retrospective and perspective. In: Advances in Engineering Technology. Ed. Jaivir Sindh, Vol. 4, Ch. 7. New Delhi: AkiNik Publications, 101-132

[14] Trokhimchuck P. P. (2020) Some Problems of the Modeling the Optical Breakdown and Shock Processes in Nonlinear and Relaxed Optics, IJARPS, Vol. 7, Is.5, 17-30.

[15] Trokhimchuck P. P. (2023) Shork Electromagnetic Processes in Nonlinear and Relaxed Optics. In: Recent Review and Research in Physics. Ed. Jayminkumar Rajanikant Ray, S.S. Sharma, Vol. 4, ch.3. New Delhi: AkiNik Publications, 23-52.

[16] Okada T., Tomita T., Matsuo S., Hashimoto S., Ishida Y., Kiyama S., Takahashi T. (2009) Formation of periodic strain layers associated with nanovoids inside a silicon carbide single crystal induced by femtosecond laser irradiation. J. Appl. Phys., Vol. 106, 054307. – 5 p.`

[17] Okada T., Tomita T., Matsuo S., Hashimoto S., Kashino R., Ito T. (2012) Formation of nanovoids in femtosecond laser irradiated single crystal silicon carbide. Material Science Forum, Vol. 725, 19 – 22.

[18] Yablonovich E. (1971) Optical Dielectric Srength of AlkaliHalide Crystalls Obtained by Laserinduced Breakdown, Appl. Phys. Lett., Vol. 19, Is. 11, 495-497.

[19] Trokhimchuck P. P. (2023) To Question about Nature of Laser-Induced Cavitation. IJARPS, Vol. 10, Is. 5, 1 – 16.

[20] Bourne N. K. (2001) On the laser ignition and initiation of explosives. Proc. Roy. Soc. London A. Vol. 457, 1401-1426.

[21] Ballard P., Fournier J., Fabbro R., Frelat J. (1991) Residual stresses induced by laser-shocks. Journal de physiqueD IV, Colloque C3, suppl. au Journal de Physique III, Vol. 1, c3-487 – c3-494.

[22] Bourne N. K. (2001) On the laser ignition and initiation of explosive. Proc. R. Soc. Lond. A, Vol. 457, 1401–1426

[23] Wang X., Liu R., He Y., Fu Y., Wang J., Li A., Guo X., Wang M., Guo W., Zang T., 4 Shu Q., Yao Y. (2022) Determination of detonation characteristics by laser-induced plasma spectra and micro-explosion dynamics. Optics Express, Vol. 30, No. 4, 4718-4736.

[24] Blanken J., Roeland Jozef Gentil de Moor R. J. G., Meire M., Verdaasdonk R. (2009) Laser Induced Explosive Vapor and Cavitation Resulting in Effective Irrigation of the Root Canal. Part 1: A Visualization Study, Lasers in Surgery and Medicine, Vol. 41,514–519

[25] Blanken J., Roeland Jozef Gentil de Moor R. J. G., Meire M., Verdaasdonk R. (2009) Laser Induced Explosive Vapor and Cavitation Resulting in Effective Irrigation of the Root Canal. Part 2: Evaluation of the Efficacy, Lasers in Surgery and Medicine, Vol. 41, 520–523

[26] Eickmans J. H., Hsieh W.-F., Chang R. K. (1987) Laser-induced explosion of H_2O droplets: spatially resolved spectra. Optics Letters, Vol. 12, No. 1, 22-24.

[27] Sano Y., Akita K., Sano T. (2020) A Mechanism for Inducing Compressive Residual Stresses on a Surface by Laser Peening without Coating. Metals, Vol. 10, is. 816, 12 p.

[28] Chaban V. V., Pal S., Prezhdo O. V. (2016) Laser-Induced Explosion of Nitrated Carbon Nanotubes: NonAdiabatic and Reactive Molecular Dynamics Simulations. J. Am. Chem. Soc., 19 November, 24 p.

[29] Gagliano F. P., Paek U. C. (1974) Observation of Laser-induced Explosion of Solid Materials and Correlation with Theory, Applied Optics, Vol. 13, No. 2, 274-279.

[30] Miotello A., Kelly R. (1999) Appl. Phys. A 69 [Suppl.], S67–S73

[31] Dolya S. N., Dolya S. S. (2012) Method of creation of directed explosion. Patent RU 2 498 199 C1, 11 p. (In Russian)

[32] Veyko V. P., Libenson M. N., Chervyakov G. G., Yakovlev E. B. (2008) Interaction laser irradiation and matter. Force optics, Phyzmatlit, Moscow (In Russian)

[33] Trokhimchuck P. P. (2020) Nonllinear Dynamical Systems. 2-nd ed. Vezha-Print, Lutsk (In Ukrainian)

[34] Zverev V.A., Solovieva N.M. (1967) On the mechanisms of destruction of ruby and leucosapphire crystals by powerful laser radiation. ZhETP, 1967, Vol. 53, Is. 6(12), 1849 – 1856 (In Russian)

[35 Atomic bomb, fission device. https://www.britannica.com/technology/atomic-bomb

[36] Williams F.A. (1985) Combustion Theory. 2nd Edition, Benjamin Cummings, California.

Citation: *Petro P. Trokhimchuck (2023) "To Question about Nature of Laser-Induced Explosive Processes and Phenomena" International Journal of Advanced Research in Physical Science (IJARPS) 10(7), pp.5-20, 2023.*